Density Functional Theoretical Studies of the Re−Xe Bonds in $Re(Cp)(CO)(PF_3)Xe$ and $Re(Cp)(CO)_2Xe$

J. McMaster,*,† P. Portius,† G. E. Ball,‡ J. P. Rourke,§ and M. W. George†

School of Chemistry, University of Nottingham, University Park, Nottingham NG7 2RD, United Kingdom, School of Chemistry, University of New South Wales, Sydney 2052, Australia, and Department of Chemistry, University of Warwick, Coventry CV4 7AL, United Kingdom

Received June 2, 2006

Density functional calculations have been used to probe the electronic structures of $Re(Cp)(CO)_2Xe$ and $Re(Cp)(CO)(PF_3)Xe$. The calculated CO stretching frequencies compare favorably with those determined experimentally. Our calculations of δ_{Xe} and $^3J_{Xe-F}$ for $Re(Cp)(CO)(PF_3)Xe$ represent the first for a well-characterized transition metal−noble gas compound and demonstrate that DFT using the BP86 and SAOP functionals reproduces these parameters to within 1% and 8% of their experimentally determined values. The calculated Re−Xe bond dissociation energies for $Re(Cp)(CO)_2Xe$ (12.3 kcal mol^{-1}) and $Re(Cp)(CO)(PF_3)Xe$ (11.9 kcal mol^{-1}) are also in excellent agreement with the lower limits for these energies estimated from the activation parameters for the reaction of the complexes with CO in supercritical Xe. A topological analysis of the electron density in $Re(Cp)(CO)_2Xe$ and $Re(Cp)(CO)(PF_3)Xe$ reveals positive $\nabla^2\rho(\mathbf{r})$ at the critical points ($\nabla^2\rho(\mathbf{r}_c) = 0.1310$ and 0.1396 e Å^5 for $Re(Cp)(CO)_2Xe$ and $Re(Cp)(CO)(PF_3)Xe$, respectively, indicating that the Re−Xe interaction is essentially closed-shell in both complexes. Fragment and overlap density of states analyses show that the orbital interactions in these compounds is dominated by overlap involving the Xe p orbitals and the orbitals of the Cp, CO, and/or PF_3 ligands; the Re d orbitals appear to contribute little to the orbital interactions between the $Re(Cp)(CO)_2$ and $Re(Cp)(CO)(PF_3)$, and Xe fragments.

Introduction

The isolation of $[AuXe_4]^{2+}[Sb_2F_{11}]^-{}_2$, $[(F_3As)AuXe]^+[Sb_2F_{11}]^-$, and $[HgXe]^{2+}[SbF_6]$-$[Sb_2F_{11}]^-$ and their characterization by X-ray crystallography have provided the first crystallographic evidence of transition metal−noble gas bonds within discrete transition metal complexes.[1,2] Previous studies of the photolyses of $Fe(CO)_5$ and $M(CO)_6$ (M = Cr, Mo, or W) in noble gas matrices had indicated that transition metal−noble gas bonds can form; on photolysis these compounds generate $Fe(CO)_4$ and $M(CO)_5$ (M = Cr, Mo, or W), respectively, which are sufficiently reactive to form complexes with Xe at 12 K.[3,4] Since then, a range of organometallic−noble gas compounds[5] have been observed in matrices,[6−22] in liquefied noble gases at cryogenic temperatures,[23−32] in the gas phase,[33−35] and in supercritical fluids[31,32,36−43] at room temperature. The first early transition metal−noble gas complex to be observed in a solution of liquefied noble gas was $Cr(CO)_5Xe$. This compound was generated by the continuous UV photolysis of $Cr(CO)_6$ dissolved in liquefied Xe (liq Xe) at 175 K or liquefied Kr (liq Kr) doped with 5% Xe at 151 K.[23] This work was followed by detailed rapid-scan FTIR studies of $M(CO)_6$ (M = Cr or W) in liq Xe and liq Kr[25] in which variable-temperature kinetics provided an estimate of the W−Xe bond dissociation energy in these compounds ($\Delta H_{W-Xe} \approx 8.4 \pm 0.2$ kcal mol^{-1}). Subsequent fast time-resolved infrared (TRIR) measurements of the CO substitution kinetics in the gas phase of $M(CO)_5Xe$ have also provided estimates of the bond dissociation energy of M−Xe in $M(CO)_5Xe$ (M = Cr, Mo, or W; M−Xe ≈ 9.0 kcal mol^{-1}).[33] Transition metal−noble gas complexes have been observed in solution through laser-based time-resolved infrared (TRIR)

* Corresponding author. E-mail: j.mcmaster@nottingham.ac.uk.
† University of Nottingham.
‡ University of New South Wales.
§ University of Warwick.

(1) Seidel, S.; Seppelt, K. *Science* **2000**, *290*, 117.
(2) Hwang, I. C.; Seidel, S.; Seppelt, K. *Angew. Chem., Int. Ed.* **2003**, *42*, 4392.
(3) Poliakoff, M.; Turner, J. J. *J. Chem. Soc., Dalton Trans.* **1974**, 2276.
(4) Perutz, R. N.; Turner, J. J. *J. Am. Chem. Soc.* **1975**, *97*, 4791.
(5) Grills, D. C.; George, M. W. *Adv. Inorg. Chem.* **2001**, *52*, 113.
(6) Church, S. P.; Poliakoff, M.; Timney, J. A.; Turner, J. J. *Inorg. Chem.* **1983**, *22*, 3259.
(7) Fairhurst, S. A.; Morton, J. R.; Perutz, R. N.; Preston, K. F. *Organometallics* **1984**, *3*, 1389.
(8) Horton-Mastin, A.; Poliakoff, M. *Organometallics* **1986**, *5*, 405.
(9) Brookhart, M.; Chandler, W.; Kessler, R. J.; Liu, Y.; Pienta, N. J.; Santini, C. C.; Hall, C.; Perutz, R. N.; Timney, J. A. *J. Am. Chem. Soc.* **1992**, *114*, 3802.
(10) Mawby, R. J.; Perutz, R. N.; Whittlesey, M. K. *Organometallics* **1995**, *14*, 3268.
(11) Virrels, I. G.; Nolan, T. F.; George, M. W.; Turner, J. J. *Organometallics* **1997**, *16*, 5879.
(12) Bays, J. T.; Bitterwolf, T. E.; Lott, K. A.; Ollino, M. A.; Rest, A. J.; Smith, L. A. *J. Organomet. Chem.* **1998**, *75*, 1389.
(13) Li, J.; Bursten, B. E.; Liang, B. Y.; Andrews, L.; Liang, B. Y.; Andrews, L.; Li, J.; Bursten, B. E. *J. Am. Chem. Soc.* **2003**, *295*, 2242.
(14) Andrews, L.; Liang, B. Y.; Li, J.; Bursten, B. E. *J. Am. Chem. Soc.* **2003**, *125*, 3126.
(15) Liang, B. Y.; Andrews, L.; Li, J.; Bursten, B. E. *Chem. Eur. J.* **2003**, *9*, 4781.
(16) Liang, B. Y.; Andrews, L.; Li, J.; Bursten, B. E. *Inorg. Chem.* **2004**, *43*, 882.
(17) Andrews, L.; Liang, B. Y.; Li, J.; Bursten, B. E. *New J. Chem.* **2004**, *28*, 289.
(18) Li, J.; Bursten, B. E.; Andrews, L.; Marsden, C. J. *J. Am. Chem. Soc.* **2004**, *126*, 3424.
(19) Wang, X. F.; Andrews, L.; Li, J.; Bursten, B. E. *Angew. Chem., Int. Ed.* **2004**, *43*, 2554.
(20) Zhao, Y. Y.; Wang, G. J.; Chen, M. H.; Zhou, M. F. *J. Phys. Chem. A* **2005**, *109*, 6621.
(21) Zhao, Y. Y.; Gong, Y.; Chen, M. H.; Ding, C. F.; Zhou, M. F. *J. Phys. Chem. A* **2005**, *109*, 11765.
(22) Zhao, Y. Y.; Gong, Y.; Chen, M. H.; Zhou, M. F. *J. Phys. Chem. A* **2006**, *110*, 1845.

10.1021/om060485l CCC: $33.50
Publication on Web 09/30/2006

spectroscopic investigations of alkane C−H activation in liq Xe and liq Kr by LM(CO)$_2$ complexes [L = (η^5-C$_5$Me$_5$), Tp*, and Bp*; Tp* = hydrotris(3,5-dimethylpyrazolyl)borate; Bp* = dihydrobis(3,5-dimethylpyrazolyl)borate]. These LM(CO)-Ng complexes have included Rh(η^5-C$_5$Me$_5$)(CO)Ng (Ng = Kr and Xe),[24,26,27] (κ^3-Tp*)Rh(CO)Xe, (κ^2-Tp*)Rh(CO)Xe, and Bp*Rh(CO)Xe.[30]

Hartree−Fock, hybrid DFT, DFT, and MP2 theoretical studies, targeted at reproducing the experimentally derived geometries and bond dissociation energies, have accompanied the synthetic, X-ray crystallographic, and UV/vis and IR spectroscopic studies of these transition metal−noble gas compounds.[44,45] The calculations on [AuXe$_4$]$^{2+}$ [44] and M(CO)$_5$Xe[45] provide geometries and estimates of the bond dissociation energies that are in good agreement with experiment and have also provided a basis for exploring the nature of the M−Ng bond within these compounds using fragment-based and topological analyses of the electron density. These analyses demonstrate a closed-shell interaction for the M−Ng bond in [AuXe$_4$]$^{2+}$ and M(CO)$_5$Xe.

Previously, we used TRIR spectroscopy to probe systematically the reactivity of M(Cp)(CO)nXe (M = Rh, n = 1; M = Mn, Re, n = 2 or M = Ta, Nb, n = 3) in supercritical Xe and Kr at room temperature. We have also shown that Re(Cp)-(CO)$_2$Xe is long-lived at room temperature in supercritical Xe solution[37] and possesses a half-life of up to 3.5 min at 170 K in liq Xe.[31] These relatively long lifetimes have enabled us to probe these complexes by NMR and FTIR spectroscopies. Thus, we obtained the ^{19}F, ^{31}P, and ^{129}Xe chemical shifts and coupling constants for Re(^{iPr}Cp)(CO)(PF$_3$)Xe and IR spectroscopic data for Re(^{iPr}Cp)(CO)(PF$_3$)Xe, Re(^{i}Pr-Cp)(CO)$_2$Xe, Re(Cp)(CO)-(PF$_3$)Xe, and Re(Cp)(CO)$_2$Xe.[32] These experimental data provide an interesting challenge for modern DFT methods and can serve to calibrate and assess the validity of these theoretical approaches in providing accurate descriptions of the electronic structures of these compounds. In this paper we apply relativistic DFT methods to (i) assess the ability of modern DFT methods to reproduce features of the experimentally determined ^{19}F, ^{31}P, and ^{129}Xe NMR parameters and IR features in Re(Cp)(CO)$_2$Xe and Re(Cp)(CO)(PF$_3$)Xe and (ii) examine the nature of the Re−Xe bond in Re(Cp)(CO)$_2$Xe and Re(Cp)(CO)(PF$_3$)Xe.

Computational Details

The calculations were performed using the Amsterdam Density Functional (ADF) suite version 2005.01.[46,47] The restricted relativistic DFT calculations employed a Slater type orbital (STO) triple-ζ plus one polarization function basis set from the ZORA/TZP database of the ADF suite for all atoms except Re, Xe, and P. All-electron basis sets were employed. For Re, Xe, and P triple-ζ plus two polarization functions (ZORA/TZ2P) all-electron basis sets were used. Scalar relativistic (SR) approaches were used within the ZORA Hamiltonian for the inclusion of relativistic effects. The local density approximation (LDA) with the correlation potential due to Vosko et al. was used in all of the DFT calculations.[48] Gradient corrections were performed using the functionals of Becke[49] and Perdew[50] (BP). Models of CpRe(CO)$_3$ and CpRe-(CO)$_2$Xe were geometry optimized in C_s symmetry, whereas CpRe-(CO)(PF$_3$)Xe was optimized without any symmetry restraints.

NMR chemical shift and coupling calculations used the geometry-optimized coordinates from the calculations above. These calculations employed a Slater type orbital (STO) triple-ζ plus two polarization functions basis set from the ZORA/TZ2P database of the ADF suite for all atoms except Re and Xe. All-electron basis sets were employed. For Re and Xe quadruple-ζ plus four polarization functions (ZORA/QZ4P) all-electron basis sets were employed. Scalar relativistic (SR) approaches were used within the ZORA Hamiltonian for the inclusion of relativistic effects. The local density approximation (LDA) with the correlation potential due to Vosko et al. was used in all of the DFT calculations.[48] Gradient corrections were performed using the functionals of Becke[49] and Perdew[50] (BP86). The absolute shielding constants (σ) for Xe, P, and F in CpRe(CO)(PF$_3$)Xe were calculated using the NMR component of the ADF suite using densities derived from the BP86 and the statistical average of orbital-dependent model potentials (SAOP) models.[51,52] The chemical shifts for Xe and F (δ) were determined from

$$\delta = \sigma_{ref} - \sigma \text{ ppm} \quad (1)$$

where σ_{ref} are the absolute shielding constants calculated for XeOF$_4$ and CFCl$_3$, respectively, at the BP86 and SAOP levels. The experimental ^{31}P reference (85% phosphoric acid) is not suitable for direct theoretical comparisons. Therefore we employed the procedure of van Wüllen[53] for the calculation of the ^{31}P chemical

(23) Simpson, M. B.; Poliakoff, M.; Turner, J. J.; Maier, W. B., II; McLaughlin, J. G. *J. Chem. Soc., Chem. Commun.* **1983**, 1355.
(24) Weiller, B. H.; Wasserman, E. P.; Bergman, R. G.; Moore, C. B.; Pimentel, G. C. *J. Am. Chem. Soc.* **1989**, *111*, 8288.
(25) Weiller, B. H. *J. Am. Chem. Soc.* **1992**, *114*, 10910.
(26) Schultz, R. H.; Bengali, A. A.; Tauber, M. J.; Weiller, B. H.; Wasserman, E. P.; Kyle, K. R.; Moore, C. B.; Bergman, R. G. *J. Am. Chem. Soc.* **1994**, *116*, 7369.
(27) Bengali, A. A.; Arndtsen, B. A.; Burger, P. M.; Schultz, R. H.; Weiller, B. H.; Kyle, K. R.; Moore, C. B.; Bergman, R. G. *Pure Appl. Chem.* **1995**, *67*, 281.
(28) Weiller, B. H.; Wasserman, E. P.; Moore, C. B.; Bergman, R. G. *J. Am. Chem. Soc.* **1993**, *115*, 4326.
(29) Bengali, A. A.; Schultz, R. H.; Moore, C. B.; Bergman, R. G. *J. Am. Chem. Soc.* **1994**, *116*, 9585.
(30) Yeston, J. S.; McNamara, B. K.; Bergman, R. G.; Moore, C. B. *Organometallics* **2000**, *19*, 3442.
(31) Childs, G. I.; Colley, C. S.; Dyer, J.; Grills, D. C.; Sun, X. Z.; Yang, J. X.; George, M. W. *J. Chem. Soc., Dalton Trans.* **2000**, 1901.
(32) Ball, G. E.; Darwish, T. A.; Geftakis, S.; George, M. W.; Lawes, D. J.; Portius, P.; Rourke, J. P. *Proc. Natl. Acad. Sci.* **2005**, *102*, 1853.
(33) Wells, J. R.; Weitz, E. *J. Am. Chem. Soc.* **1992**, *114*, 2783.
(34) Zheng, Y.; Wang, W.; Lin, J.; She, Y.; Fu, K. J. *J. Phys. Chem.* **1992**, *96*, 7650.
(35) Jyo-O, M.; Takeda, H.; Omiya, K.; Ishikawa, Y.; Arai, S. *Bull. Chem. Soc. Jpn.* **1993**, *66*, 3618.
(36) Sun, X. Z.; George, M. W.; Kazarian, S. G.; Nikiforov, S. M.; Poliakoff, M. *J. Am. Chem. Soc.* **1996**, *118*, 10525.
(37) Sun, X. Z.; Grills, D. C.; Nikiforov, S. M.; Poliakoff, M.; George, M. W. *J. Am. Chem. Soc.* **1997**, *119*, 7521.
(38) Grills, D. C.; Sun, X. Z.; Childs, G. I.; George, M. W. *J. Phys. Chem. A* **2000**, *104*, 4300.
(39) Grills, D. C.; Childs, G. I.; George, M. W. *Chem. Commun.* **2000**, 1841.
(40) Childs, G. I.; Grills, D. C.; Sun, X. Z.; George, M. W. *Pure Appl. Chem.* **2001**, *73*, 443.
(41) Sun, X. Z.; Nikiforov, S. M.; Yang, J.; Colley, C. S.; George, M. W. *Appl. Spectrosc.* **2002**, *56*, 31.
(42) Jina, O. S.; Sun, X. Z.; George, M. W. *Dalton Trans.* **2003**, 1773.
(43) Kuimova, M. K.; Alsindi, W. Z.; Dyer, J.; Grills, D. C.; Jina, O. S.; Matousek, P.; Parker, A. W.; Portius, P.; Sun, X. Z.; Towrie, M.; Wilson, C.; Yang, J.; George, M. W. *Dalton Trans.* **2003**, 3996.
(44) Berski, S.; Latajka, Z.; Andrés, J. *Chem. Phys. Lett.* **2002**, *356*, 483.
(45) Ehlers, A. W.; Frenking, G.; Baerends, E. J. *Organometallics* **1997**, *16*, 4896.
(46) Fonseca Guerra, C.; Snijders, J. G.; te Velde, G.; Baerends, E. J. *Theor. Chem. Acc.* **1998**, *99*, 391.
(47) te Velde, G.; Bickelhaupt, F. M.; van Gisbergen, S. J. A.; Fonseca Guerra, C.; Baerends, E. J.; Snijders, J. G.; Ziegler, T. *J. Comput. Chem.* **2001**, *22*, 931.
(48) Vosko, S. H.; Wilk, L.; Nusair, M. *Can. J. Phys.* **1980**, *58*, 1200.
(49) Becke, A. D. *Phys. Rev. A* **1988**, *38*, 3098.
(50) Perdew, J. P. *Phys. Rev. B* **1986**, *33*, 8822.
(51) Poater, J.; van Lenthe, E.; Baerends, E. J. *J. Chem. Phys.* **2003**, *118*, 8584.
(52) Schipper, P. R. T.; Gritsenko, O. V.; van Gisbergen, S. J. A.; Baerends, E. J. *J. Chem. Phys.* **2000**, *112*, 1344.
(53) van Wüllen, Ch. *Phys. Chem. Chem. Phys.* **2000**, *2*, 2137.

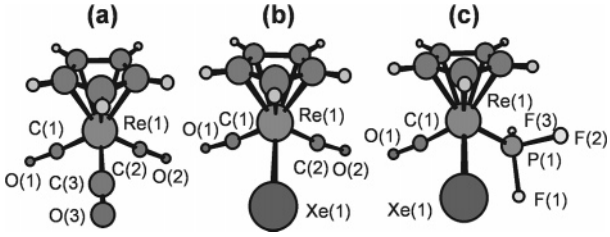

Figure 1. Geometry-optimized structures of (a) $Re(Cp)(CO)_3$, (b) $Re(Cp)(CO)_2Xe$, and (c) $Re(Cp)(CO)(PF_3)Xe$.

shift. The calculated absolute shieldings are converted to the NMR chemical shifts such that the experimental gas-phase chemical shift of PH_3 (−266.1 ppm[54]) is reproduced exactly. Thus,

$$\delta_P = \sigma(PH_3, \text{calcd}) - \sigma - 266.1 \text{ ppm} \quad (2)$$

$^2J_{Xe-P}$, J_{P-F}, and $^3J_{Xe-F}$ coupling constants were calculated using the CPL component of the ADF suite.

In addition to gas-phase calculations of the NMR absolute shieldings and spin−spin couplings we performed solvent-based calculations using COSMO (conductor-like screening model)[55,56] as implemented in ADF[46,47] to treat the Xe solvent as a polarizable continuum. We used the van der Waals radii of the component atoms to construct the solvent cavity and an experimentally determined dielectric constant ($\epsilon = 1.66$) for supercritical xenon.[57] The Kohn−Sham orbitals were created using the MOLEKEL[58] visualization package, and the bonding within the molecules was analyzed using the AOMIX package.[59,60]

Results and Discussion

Figure 1 shows the optimized geometries and atom labeling of $Re(Cp)(CO)_3$, $Re(Cp)(CO)_2Xe$, and $Re(Cp)(CO)(PF_3)Xe$, and Table 1 lists selected bond lengths and angles for these complexes.

The DFT geometry optimization of $Re(Cp)(CO)_3$ successfully reproduces the principal features of the structure of $Re(Cp)(CO)_3$ as determined by X-ray crystallography;[61] the average $C_{carbonyl}-Re(1)-C_{carbonyl}$ and $C_{carbonyl}-Re(1)-Cp(centroid)$ angles are similar in the experimental (90.0° and 125.3°) and calculated (90.5° and 124.9°) geometries, and the $Re(1)-C_{carbonyl}$, C−O, and Re(1)−Cp(centroid) distances are ca. 0.025, 0.010, and 0.045 Å longer, respectively, in the calculated structure. Thus, these scalar relativistic calculations appear to provide good estimates of the geometry of $Re(Cp)(CO)_3$ and place some confidence on the reliability of the calculated structures for $Re(Cp)(CO)_2Xe$ and $Re(Cp)(CO)(PF_3)Xe$, for which no X-ray crystallographic data are available. For the $Re(Cp)(CO)_2Xe$ and $Re(Cp)(CO)(PF_3)Xe$ model geometries, the calculated $Re(1)-C_{carbonyl}$ and Re(1)−Cp(centroid) distances are shorter and the C−O distances are longer than those of $Re(Cp)(CO)_3$, consistent with the increase in the Re → CO and Cp back-bonding that results from the replacement of one CO ligand by Xe. The ligand bond angles remain essentially invariant across the $Re(Cp)(CO)_3$, $Re(Cp)(CO)_2Xe$, and $Re(Cp)(CO)(PF_3)Xe$ geometries, indicating that the perturbations in geometry, accompanying the exchange of Xe for CO in $Re(Cp)(CO)_3$, lie principally along existing Re−ligand vectors.

Table 2 shows a comparison between the energies of the calculated and experimental CO stretching vibrations for $Re(Cp)(CO)_3$, $Re(Cp)(CO)_2Xe$, and $Re(Cp)(CO)(PF_3)Xe$. The calculated harmonic CO stretching energies are ca. 21−36 cm^{-1} lower than the observed fundamental wavenumbers, an offset that is comparable to that derived from DFT calculations at the BP86/ECP2 level on $M(CO)_6$ (M = Cr, Mo, W), $M(CO)_5$ (M = Fe, Ru, Os), and $M(CO)_4$ (M = Ni, Pd, Pt), for which experimental gas-phase spectroscopic data are available.[62−64] For these compounds an optimum offset of 28.3 cm^{-1} for the CO stretching vibrations was calculated, leading to a rms deviation $\delta_{rms} = 5.6$ cm^{-1} for the energies of the CO stretching vibrations predicted at the BP86/ECP2 level.[63] The trends in the energies of the CO stretching vibrations of $Re(Cp)(CO)_3$, $Re(Cp)(CO)_2Xe$, and $Re(Cp)(CO)(PF_3)Xe$, Table 2, are consistent with the structural variations observed in the geometry-optimized structures.

Table 2 shows the calculated NMR parameters for $Re(Cp)(CO)(PF_3)Xe$ employing the BP86 and SAOP potentials and an all-electron ZORA/TZ2P basis set for all atoms except Xe and Re, for which we used the all-electron ZORA/QZ4P basis set. We employed the optimized $Re(Cp)(CO)(PF_3)Xe$ model geometry calculated as described above. The fluid solution ^{19}F NMR spectrum of $Re(^{iPr}Cp)(CO)(PF_3)Xe$[32] shows a single doublet of doublets resulting from coupling to the ^{31}P and ^{129}Xe nuclei, indicating that each ^{19}F resonance within the PF_3 unit is rotationally averaged. Thus, estimates of the calculated δ_F, J_{P-F}, and $^3J_{Xe-F}$ parameters were made by averaging the calculated values for each ^{19}F nucleus within the static model derived from geometry optimizations. Calculations employing the BP86 potential reproduce the magnitude of the experimental[32] δ_{Xe} and $^3J_{Xe-F}$ parameters of $Re(^{iPr}Cp)(CO)(PF_3)Xe$, Table 2. We also employed the SAOP potential[51] in our calculations of the NMR parameters of $Re(Cp)(CO)(PF_3)Xe$. This potential has been shown to offer considerable improvements in the prediction of static and frequency-dependent molecular response properties over the LDA and GGA potentials, particularly for C, H, N, and F nuclei.[51] For $Re(^{iPr}Cp)(CO)(PF_3)Xe$, the SAOP potential offers good estimates of the δ_{Xe} and $^3J_{Xe-F}$ parameters, each being within 1% and 8%, respectively, of their experimental values, Table 2. However, estimates of δ_P and δ_F show little or no improvement. Therefore we probed the effect of a supercritical Xe solvent continuum using a COSMO model at the BP86 and SAOP levels in an attempt to improve the correspondence between the calculated and experimental δ_P and δ_F chemical shifts, Table 2. Embedding $Re(^{iPr}Cp)(CO)(PF_3)Xe$ in Xe as solvent led to little change in the polarization of the P−F bond, as measured by the atomic charges of the P and F nuclei, Table 2, and consequently little change in the chemical shifts of these nuclei relative to $Re(^{iPr}Cp)(CO)(PF_3)Xe$ in the gaseous state.

It has been argued previously that a straightforward application of eq 1 to the conversion of theoretical absolute shieldings to chemical shifts tends to bias comparisons by assigning an

(54) Zilm, K. W.; Webb, G. G.; Cowley, A. H.; Pakulski, M.; Orendt, A. *J. Am. Chem. Soc.* **1988**, *110*, 2032.
(55) Klamt, A.; Schüürmann, G. *J. Chem. Soc., Perkin Trans. 2* **1993**, 799.
(56) Pye, C. C.; Ziegler, T. *Theor. Chem. Acc.* **1999**, *101*, 396.
(57) Fulton, J. L.; Blitz, J. P.; Tingey, J. M.; Smith, R. D. *J. Phys. Chem.* **1989**, *93*, 4198.
(58) Flükiger, P.; Lüthi, H. P.; Portmann, S.; Weber, J. *MOLEKEL 4.0 Swiss Center for Scientific Computing*; Manno (Switzerland), 2000.
(59) Gorelsky, S. I. *AOMix Program*; 2001, http://www.sg-chem.net.
(60) Gorelsky, S. I.; Lever, A. B. P. *J. Organomet. Chem.* **2001**, *635*, 187.
(61) Fitzpatrick, P. J.; Le Page, Y.; Butler, I. S. *Acta Crystallogr., Sect. B* **1981**, *37*, 1052.
(62) Jonas, V.; Thiel, W. *J. Chem. Phys.* **1995**, *102*, 8474.
(63) Jonas, V.; Thiel, W. *Organometallics* **1998**, *17*, 353.
(64) Spears, K. G. *J. Phys. Chem. A* **1997**, *101*, 6273.

Table 1. Geometrical Parameters for Re(Cp)(CO)$_3$, Re(Cp)(CO)$_2$Xe, and Re(Cp)(CO)(PF$_3$)Xe

	Re(Cp)(CO)$_3$ (experimental)[61]	Re(Cp)(CO)$_3$ (calculated)	Re(Cp)(CO)$_2$Xe (calculated)	Re(Cp)(CO)(PF$_3$)Xe (calculated)
		Distances/Å		
Re(1)−C(1)	1.888(7)	1.919	1.899	1.903
Re(1)−C(2)	1.899(7)	1.919	1.899	
Re(1)−C(3)	1.894(8)	1.919		
C(1)−O(1)	1.159(9)	1.170	1.178	1.178
C(2)−O(2)	1.160(9)	1.170	1.178	
C(3)−O(3)	1.162(10)	1.170		
Re(1)−Xe(1)			2.910	2.901
Re(1)−P(1)				2.209
Re−Cp(centroid)	1.957	2.003	1.948	1.939
		Angles/deg		
C(1)−Re(1)−C(2)	89.4(3)	90.7	90.3	
C(1)−Re(1)−C(3)	90.5(3)	90.4		
C(2)−Re(1)−C(3)	90.1(4)	90.4		
C(1)−Re(1)−Xe(1)			92.1	92.6
C(2)−Re(1)−Xe(1)			92.1	
C(1)−Re(1)−P(1)				89.4
Xe(1)−Re(1)−P(1)				93.0
Cp(centroid)−Re−L(average)	125.3	124.9	124.2	123.6

Table 2. Calculated and Experimental ν_{CO} and δ_{Xe}, δ_P, and δ_F for Re(Cp)(CO)$_3$, Re(Cp)(CO)$_2$Xe, and Re(Cp)(CO)(PF$_3$)Xe

	method	ν_{CO} (calc)/cm^{-1}	ν_{CO} (exptl)/cm^{-1}	δ_{Xe} /ppm	δ_P /ppm	δ_F /ppm	$^2J_{Xe-P}$ /Hz	J_{P-F} /Hz	$^3J_{Xe-F}$ /Hz	atomic charge P	average atomic charge F
Re(Cp)(CO)$_3$	BP86 TZ2P(Re,Xe)/TZP	1921 1922 1996	1946[a] 2035[a]								
Re(Cp)(CO)$_2$Xe	BP86 TZ2P(Re,Xe)/TZP	1873 1924	1894[a] 1957[a]								
	BP86 TZ2P(Re,Xe)/TZP	1900	1924[b]								
	BP86 QZ4P(Re,Xe)/TZ2P			−6595	161	−29	−37.9	−1406.7	9.5	1.4063	−0.4545
	BP86, COSMO QZ4P(Re,Xe)/TZ2P			−6608	167	−24	−36.2	−1395.9	9.5	1.4291	−0.4639
Re(Cp)(CO)(PF$_3$)Xe	SAOP QZ4P(Re,Xe)/TZ2P			−6224	85	−42	−38.3	−1267.3	7.3	1.7049	−0.5557
	SAOP, COSMO QZ4P(Re,Xe)/TZ2P			−6241	83	−42	−36.4	−1275.4	7.3	1.7293	−0.5644
	exptl NMR params for Re(^{iPr}Cp)(CO)(PF$_3$)Xe			−6179 ± 3	114	−5.1	41.8 ± 1	1216	5.1 ± 0.8		

[a] Recorded in scXe at 298 K. [b] Recorded in lXe at 166 K.[32]

excessive significance to the error in the calculated absolute shielding of the reference nucleus.[51,65,66] Therefore σ_{ref} has previously been treated as an adjustable parameter, chosen to eliminate the average signed error in the calculated chemical shifts. A statistically significant set of theoretical calculations have been performed for molecules containing C, H, N, O, and F nuclei to assess the average absolute errors in chemical shifts and to adjust the reference chemical shieldings for these nuclei. The BP86 and SAOP functionals yield average absolute errors in the chemical shifts of molecules containing ^{19}F nuclei of 20.4 and 17.6 ppm, respectively. Similar calculations for molecules containing ^{31}P atoms yield an average absolute error in δ_P of 33.0 ppm for the self-interaction-free, gradient-corrected SIC-VWN functional.[65] The errors in the calculated δ_F and δ_P for Re(Cp)(CO)(PF$_3$)Xe are comparable to those reported for these previous calculations. This suggests that the differences in the calculated and experimental δ_F and δ_P for Re(Cp)(CO)(PF$_3$)Xe and Re(^{iPr}Cp)(CO)(PF$_3$)Xe may result from errors in the calculated absolute shielding of the reference nuclei. Nevertheless, the excellent agreement between the calculated and experimental δ_{Xe} and $^3J_{Xe-F}$ parameters suggests that the SAOP potential provides an excellent model for the calculation of transition metal−Xe NMR parameters.

Table 3 shows predicted Re(1)−Xe(1) bond energies in Re(Cp)(CO)$_2$Xe and Re(Cp)(CO)(PF$_3$)Xe associated with reactions 1 and 2.

$$\text{Re(Cp)(CO)}_2\text{Xe} \rightarrow \text{Re(Cp)(CO)}_2 + \text{Xe} \quad (1)$$

$$\text{Re(Cp)(CO)(PF}_3\text{)Xe} \rightarrow \text{Re(Cp)(CO)(PF}_3\text{)} + \text{Xe} \quad (2)$$

The calculated bond energy (ΔE) comprises two terms:

$$\Delta E = -(\Delta E_{prep} + \Delta E_{int})$$

where ΔE_{prep} is the energy difference between the Re(Cp)(CO)$_2$ [or Re(Cp)(CO)(PF$_3$)] fragment in its equilibrium geometry and in the geometry of Re(Cp)(CO)$_2$Xe [or Re(Cp)(CO)(PF$_3$)Xe]

(65) Patchkovskii, S.; Ziegler, T. *J. Phys. Chem. A* **2002**, *106*, 1088.
(66) Patchkovskii, S.; Autschbach, J.; Ziegler, T. *J. Chem. Phys.* **2001**, *115*, 26.

Table 3. Dissociation Energies (kcal mol^{-1}) for Re(Cp)(CO)$_2$Xe and Re(Cp)(CO)(PF$_3$)Xe

	ΔE_{prep}	ΔE_{int}	ΔE_{Pauli}	ΔE_{El}	ΔE_{Orb}	ΔE	ΔH_{298}	ΔH_{298} (corrected for BSSE)	exptl $\Delta H^{\ddagger}$
Re(Cp)CO)$_2$Xe	0.4	−11.7	32.0	−21.3	−22.4	11.3	12.8	12.2	11.9 ± 0.4 11.7 ± 0.4[a]
Re(Cp)(CO)(PF$_3$)Xe	1.0	−12.3	32.7	−21.6	−23.4	11.2	12.7	11.7	– 12.4 ± 0.4[b]

[a] For Re($^{i\text{Pr}}$Cp)(CO)$_2$Xe.[32] [b] For Re($^{i\text{Pr}}$Cp)(CO)(PF$_3$)Xe.[32]

and the interaction energy, ΔE_{int}, which is the energy change when the Re(Cp)(CO)$_2$ [or Re(Cp)(CO)(PF$_3$)] and Xe fragments are combined together.

Table 3 also shows experimental estimates of the activation energies, $\Delta H^{\ddagger}$, for the reaction of Re($^{i\text{Pr}}$Cp)(CO)(PF$_3$)Xe and Re($^{i\text{Pr}}$Cp)(CO)$_2$Xe with CO.[32] Thus, the magnitude of $\Delta H^{\ddagger}$ places a lower limit on the Re(1)−Xe(1) dissociation enthalpies. We converted the calculated dissociation energies ΔE into the bond enthalpies, ΔH_{298}, using the corrections that have been described previously for M(CO)$_5$−Ng (M = Cr, Mo, W and Ng = Ar, Kr, Xe).[45] These thermal corrections for the bond dissociation reactions 1 and 2 include a work term $pV = RT$ (0.6 kcal mol^{-1}), three degrees of translation (0.9 kcal mol^{-1}), and zero-point energies [ca. 0.1 kcal mol^{-1} for Re(Cp)(CO)$_2$-Xe and Re(Cp)(CO)(PF$_3$)Xe]. Table 3 also shows ΔH_{298} corrected for basis set superposition errors (BSSEs), calculated using the counterpoise correction.[67,68] Previous studies have shown that, for weakly bound systems, BSSEs may lead to substantial overestimations of the bond energies.[69] For medium-sized basis sets (e.g., the DZ basis from the ADF database) BSSEs for M(CO)$_5$−Ng (M = Cr, Mo, W and Ng = Ar, Kr, Xe) have been shown to be of the same order of magnitude as ΔE for the M−Ng bond; the use of an extended basis set, DZP, reduces significantly the BSSE for these molecules (BSSEs are ca. 0.3−0.5 kcal mol^{-1}).[45] We have employed all-electron basis sets at the TZ2P level for Re, Xe, and P, and TZP for the remaining atoms, which yield BSSEs of 0.7 and 1.0 kcal mol^{-1} for the Re(1)−Xe(1) bond energies of Re(Cp)(CO)$_2$Xe and Re-(Cp)(CO)(PF$_3$)Xe, respectively. These BSSEs represent ca. 6−8% of ΔE, Table 3.

The calculated ΔH_{298} values lie ca. 0.3 kcal mol^{-1} outside of the experimentally determined range of $\Delta H^{\ddagger}$ for the dissociation of the Re(1)−Xe(1) bonds. This excellent agreement between the calculated ΔH_{298} and experimental $\Delta H^{\ddagger}$ values suggest that Re($^{i\text{Pr}}$Cp)(CO)$_2$Xe and Re($^{i\text{Pr}}$Cp)(CO)(PF$_3$)Xe react with CO in supercritical Xe predominantly via a dissociative mechanism. However, a cancellation of errors within the theoretical analyses (see below) may contribute to the close correspondence between the theoretical and experimental results. The calculated Re(1)−Xe(1) bond energies in Re(Cp)(CO)$_2$Xe and Re(Cp)(CO)(PF$_3$)Xe are ca. 3−4 kcal mol^{-1} higher than those of the M−Xe bonds in M(CO)$_5$Xe (M = Cr, Mo, W),[45] which mirrors the experimental observation of weaker M−Xe bonds in the latter compounds.

A topological analysis of the electron density distribution, discussed below, shows that the bonding in Re(Cp)(CO)$_2$Xe and Re(Cp)(CO)(PF$_3$)Xe is dominated by charge-induced dipole and dispersion effects. It is now clearly recognized that all gradient-corrected density functionals are unable to describe dispersive interactions, and it has proven difficult to account for dispersion within the standard Kohn−Sham framework.[70−73] New empirical approaches, which add an empirical potential of the form C_6R^{-6} to the usual DFT energy (where R are interatomic distances and C_6 are the dispersion coefficients), have appeared in an attempt to correct for dispersion effects.[73] However, these new methods have not been assessed with regard to the treatment of the bonding in transition metal−noble gas complexes. Thus, the apparent good agreement between the calculated and experimental bond energies for Re($^{i\text{Pr}}$Cp)(CO)(PF$_3$)Xe and Re-($^{i\text{Pr}}$Cp)(CO)$_2$Xe may result from error cancellation in which the BP86 functional overestimates the bonding due to charge-induced dipoles and neglects bonding due to dispersion.

We have examined the nature of the Re(1)−Xe(1) bonds in Re(Cp)(CO)$_2$Xe and Re(Cp)(CO)(PF$_3$)Xe by using a topological analysis of the electron density distribution, and its Laplacian, for the geometry-optimized structures at the TZ2P/TZP BP86

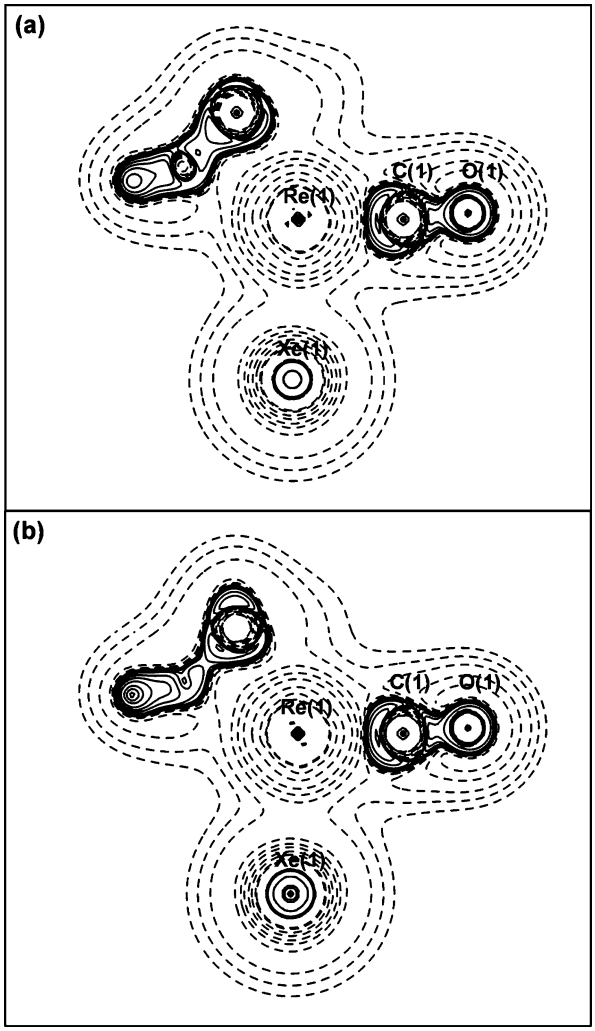

Figure 2. Contour diagram of the Laplacian distribution $\nabla^2\rho(\mathbf{r})$ of (a) Re(Cp)(CO)$_2$Xe and (b) Re(Cp)(CO)(PF$_3$)Xe. Dashed lines indicate charge depletion ($\nabla^2\rho(\mathbf{r}) > 0$); solid lines indicate charge concentration ($\nabla^2\rho(\mathbf{r}) < 0$).

(67) Boys, S. F.; Bernardi, F. *Mol. Phys.* **1979**, *37*, 1529.
(68) Rosa, A.; Ehlers, A. W.; Baerends, E. J.; Snijders, J. G.; te Velde, G. *J. Phys. Chem.* **1996**, *100*, 5690.
(69) van Lenthe, J. H.; van Rijdt, J. G. C.; van Duijneveldt, F. B. Weakly Bonded Systems. In *Ab Initio Methods in Quantum Chemistry, Part II, Adv. Chem. Phys. LXIX*; Wiley and Sons: New York, 1987.

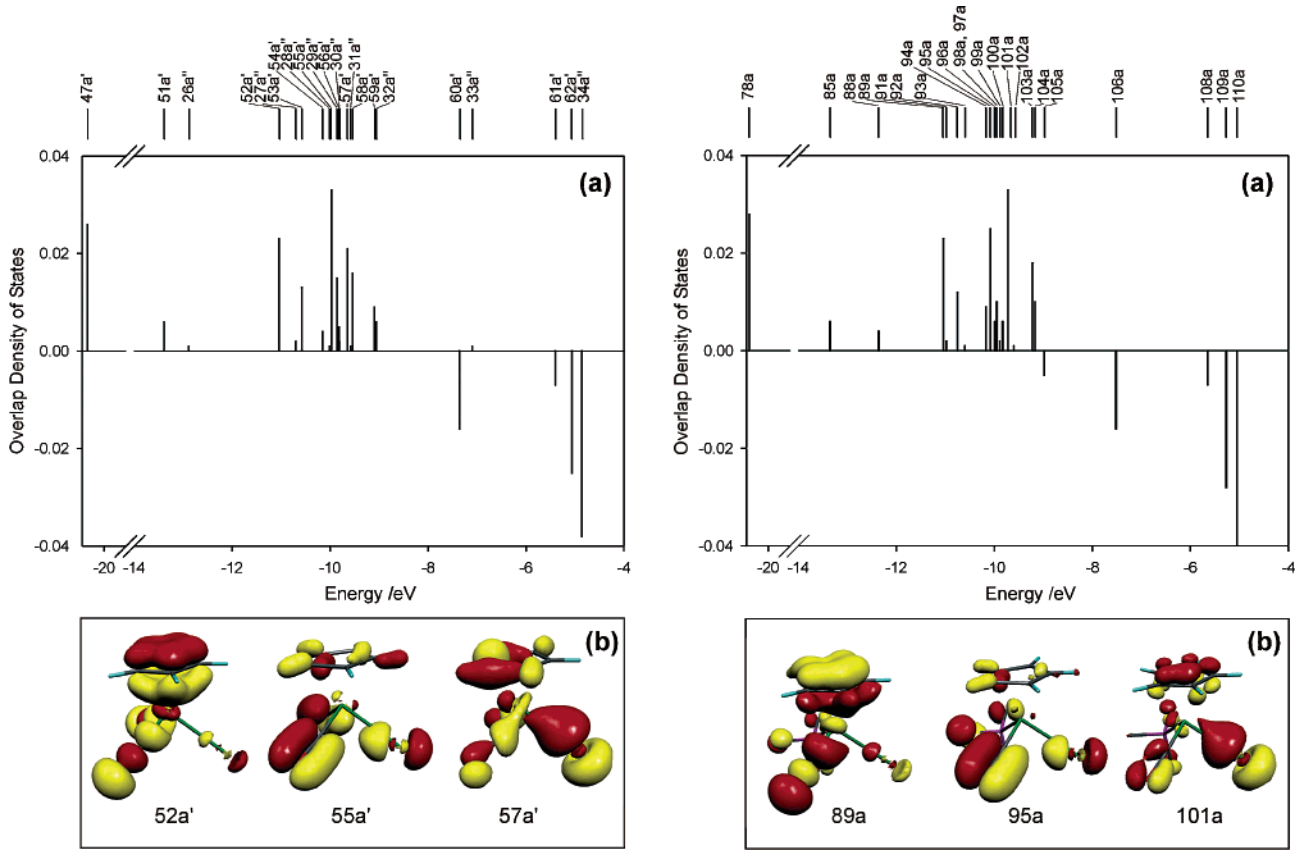

Figure 3. (a) Overlap density of states diagram for the frontier orbitals of (a) Re(Cp)(CO)$_2$Xe and (b) Re(Cp)(CO)(PF$_3$)Xe with selected plots of the principal Kohn−Sham orbitals that are bonding with respect to the Re−Xe bond shown beneath each diagram.

Table 4. Critical Point Properties for Re(Cp)(CO)$_2$Xe and Re(Cp)(CO)(PF$_3$)Xe for Electron Densities Calculated at the TZ2P/TZP BP86 Level

	$\rho(\mathbf{r}_c)$	$\nabla^2\rho(\mathbf{r}_c)$	λ_1	λ_2	λ_3	$\lvert\lambda_1\rvert/\lambda_3$
Re(Cp)(CO)$_2$Xe	0.037	0.1310	−0.02357	−0.01871	0.1733	0.136
Re(Cp)(CO)(PF$_3$)Xe	0.038	0.1396	−0.02416	−0.01748	0.1812	0.133

level. Figure 2 shows the Laplacian distributions of Re(Cp)(CO)$_2$Xe and Re(Cp)(CO)(PF$_3$)Xe within the plane defined by the Re(1), Xe(1), and C(1) atoms. The area of electron concentration ($\nabla^2\rho(\mathbf{r}) < 0$, solid lines) exhibits an approximately circular shape, which indicates that the electronic structure of the Xe atom is hardly disturbed within the complexes. This should be contrasted with the Laplacians of the electron densities between the Re(1) and C(1) atoms that show a clear electron concentration between the Re(1) and C(1) atoms.

The properties of the (3,−1) critical points are shown in Table 4, and these provide information for a density-based classification of the chemical bonding.[74,75] The positive values of the curvatures along the bond paths (λ_3) and the small, negative values of λ_1 and λ_2 contribute to positive $\nabla^2\rho(\mathbf{r})$ at the critical points ($\nabla^2\rho(\mathbf{r}_c) = 0.1310$ and 0.1396 e Å^5 for Re(Cp)(CO)$_2$Xe and Re(Cp)(CO)(PF$_3$)Xe, respectively, Table 4). This behavior is associated with little or no density accumulation within the Re(1)−Xe(1) bonds, indicating that the Re(1)−Xe(1) interaction is essentially closed-shell, i.e., charge-induced dipole and dispersive, in both complexes. This is also confirmed by the small values of $\rho(\mathbf{r}_c)$ [$\rho(\mathbf{r}_c) = 0.037$ and 0.038 for Re(Cp)(CO)$_2$Xe and Re(Cp)(CO)(PF$_3$)Xe, respectively, Table 4] for the Re(1)−Xe(1) bonds and by $|\lambda_1|/\lambda_3$, which is <1 in both cases. These parameters are similar to those of the hydrogen bond in (HF)$_2$ ($\rho(\mathbf{r}_c) = 0.0262$, $\nabla^2\rho(\mathbf{r}_c) = 0.1198$, $\lambda_1 = -0.0406$, $\lambda_2 = -0.0360$, $\lambda_3 = 0.1994$, and $|\lambda_1|/\lambda_3 = 0.204$).[64] Similar closed-shell interactions have been identified in M(CO)$_5$−Ng (M = Cr, Mo, W and Ng = Ar, Kr, Xe)[45] and [AuXe$_4$]$^{2+}$,[44] which exhibit similar Laplacian distributions to Re(Cp)(CO)$_2$Xe and Re(Cp)(CO)(PF$_3$)Xe across the M−Ng bond path.

We performed a bond energy analysis using the energy decomposition scheme as implemented in ADF to gain further insight into the Re(1)−Xe(1) bond of Re(Cp)(CO)$_2$Xe and Re(Cp)(CO)(PF$_3$)Xe. The preparation energies (ΔE_{prep}, Table 3) needed to change the equilibrium geometries of the Re(Cp)(CO)$_2$ and Re(Cp)(CO)(PF$_3$) fragments into their geometries in Re(Cp)(CO)$_2$Xe and Re(Cp)(CO)(PF$_3$)Xe represent ca. 5−10% of the bond dissociation energy (ΔE). The equilibrium geometries of both fragments are similar to the geometries in the respective complexes; the higher ΔE_{prep} for Re(Cp)(CO)(PF$_3$) relative to Re(Cp)(CO)$_2$ ($\Delta E_{prep} = 1.0$ and 0.4 kcal mol^{-1}, respectively) presumably reflects the interactions of the larger PF$_3$ ligand with the rest of the coordination sphere in Re(Cp)(CO)(PF$_3$) relative to the smaller CO ligand in Re(Cp)(CO)$_2$. The internal energy, ΔE_{int}, has contributions from the Pauli repulsions between the occupied orbitals, ΔE_{Pauli}, attractive electrostatic interactions, ΔE_{El}, and orbital interactions, ΔE_{Orb},

(70) Kristyan, S.; Pulay, P. *Chem. Phys. Lett.* **1994**, *229*, 175.
(71) Allen, M.; Tozer, D. J. *J. Chem. Phys.* **2002**, *117*, 11113.
(72) Grimme, S. *J. Comput. Chem.* **2004**, *25*, 1463.
(73) Piacenza, M.; Grimme, S. *J. Am. Chem. Soc.* **2005**, *127*, 14841.
(74) Bader, R. F. W. *Atoms in Molecules, A Quantum Theory*; Oxford University Press: Oxford, 1990.
(75) Coppens, P. *X-Ray Charge Densities and Chemical Bonding*; Oxford University Press: Oxford, 1997.

containing contributions from the donation of charge from the occupied orbitals of one fragment and the virtual orbitals of the other fragment and the mixing of occupied and virtual orbitals of the same fragment:

$$\Delta E_{int} = \Delta E_{Pauli} + \Delta E_{El} + \Delta E_{Orb}$$

Both complexes exhibit Pauli repulsions ΔE_{Pauli} of ca. 32 kcal mol^{-1}. This repulsion is compensated for by favorable ΔE_{El} and ΔE_{Orb} terms of ca. -21 and -22 kcal mol^{-1}, respectively. These terms are ca. 10 kcal mol^{-1} greater than those calculated for $W(CO)_5Xe$ ($\Delta E_{Pauli} = 20.8$, $\Delta E_{El} = -12.5$, and $\Delta E_{Orb} = -15$ kcal mol^{-1})[45] that presumably reflect the greater steric congestion, the effective Re(I) oxidation state, and the greater orbital contributions to the bonding in $Re(Cp)(CO)_2Xe$ and $Re(Cp)(CO)(PF_3)Xe$. However, we note that this bond energy decomposition scheme does not include contributions from dispersion that, as we have shown above, are expected to contribute to the bonding within these compounds.

We have performed a fragment-based analysis of the bonding in $Re(Cp)(CO)_2Xe$ and $Re(Cp)(CO)(PF_3)Xe$ to probe the orbital interactions that contribute to the Re−Xe bond. The energies and characters of the frontier orbitals of $Re(Cp)(CO)_2Xe$ and $Re(Cp)(CO)(PF_3)Xe$ are shown in Tables SI1 and SI2, and overlap population density-of-states (OPDOS) summarizing the occupied frontier orbitals of $Re(Cp)(CO)_2Xe$ and $Re(Cp)(CO)(PF_3)Xe$ are shown in Figure 3. Similar diagrams have been referred to as crystal orbital overlap population (COOP) diagrams within the literature.[76] A positive OPDOS corresponds to a bonding interaction between the $Re(Cp)(CO)_2$ or $Re(Cp)(CO)(PF_3)$ fragments with the Xe atom, whereas a negative OPDOS reveals an antibonding interaction between the metal fragment and the Xe center. Figure 3 shows clusters of orbitals between -9 and -14 eV in $Re(Cp)(CO)_2Xe$ and $Re(Cp)(CO)(PF_3)Xe$ that show a weak bonding interaction with respect to the Re−Xe bond and are the dominant contributors to the stabilization associated with ΔE_{Orb}, Table 3. These orbitals are dominated by the contributions from the Cp, CO, and PF_3 ligands, Tables SI1 and SI2, and possess little Re d orbital character (<7%). A previous analysis of the bonding in $[M(CO)_5-Ng]$ (M = Cr, Mo, W; Ng = Ar, Kr, Xe) has revealed a similar bonding scheme in which the principal bonding interaction is between the Ng-p_z orbital and an orbital dominated by the $2\pi^*$ orbitals of the CO ligands with a contribution from the M-p_z orbital.[45] A dominant contribution to ΔE_{Orb} involving a metal-based d orbital appears to be ruled out in these systems on the basis that the energy levels of the noble gas np orbitals are too low with respect to the d-transition-metal orbital manifold.[45] Thus, it appears that the contributions to ΔE_{Orb} in $Re(Cp)(CO)_2Xe$ and $Re(Cp)(CO)(PF_3)Xe$ are dominated by Xe p overlap with $Re(Cp)(CO)_2$ and $Re(Cp)(CO)(PF_3)$ fragment orbitals that are primarily Cp, CO, or PF_3 based and possess little Re d-character.

(76) Hughbanks, T.; Hoffmann, R. *J. Am. Chem. Soc.* **1983**, *105*, 3528.

Conclusions

We have established that relativistic DFT calculations provide good estimates of the geometry, ν(CO) frequencies, Re−Xe bond dissociation energies, and δ_{Xe} and $^3J_{Xe-F}$ parameters for $Re(Cp)(CO)_2Xe$ and $Re(Cp)(CO)(PF_3)Xe$. The SAOP potential offers some improvement in the agreement between the δ_{Xe} and $^3J_{Xe-F}$ parameters for $Re(Cp)(CO)(PF_3)Xe$ but little improvement in δ_P and δ_F, although the differences between experimental and calculated δ_P and δ_F lie within the range of errors previously reported for other small molecules. A topological analysis of the electron density in $Re(Cp)(CO)_2Xe$ and $Re(Cp)(CO)(PF_3)Xe$ reveals parameters that are typical of a closed-shell interaction indicative of dominant charge-induced dipole and dispersive bonding in $Re(Cp)(CO)_2Xe$ and $Re(Cp)(CO)(PF_3)Xe$. A fragment analysis reveals that the weak orbital interactions between the Xe and $Re(Cp)(CO)_2Xe$ and $Re(Cp)(CO)(PF_3)$ fragments are dominated by overlap involving the Xe p orbitals and the orbitals of the Cp, CO, and/or PF_3 ligands; the Re d orbitals appear to contribute little to the bonding interactions.

Acknowledgment. We thank the EPSRC and the Royal Society for supporting this work.

Supporting Information Available: This material is available free of charge via the Internet at http://pubs.acs.org.

OM060485L